A Method for Calculating Lower Extremity Anatomical Landmark Trajectories Based on Inertial Motion Capture Data

Zhengtao Wang, Fei Gao, Zihao Wu, Dongmei Wang, Xin Guo, and Suiran Yu

***Abstract*— Anatomical landmark trajectories are commonly used to define joint coordinate systems in human kinematic analysis according to standards proposed by the International Society of Biomechanics (ISB). However, most inertial motion capture (IMC) studies focus only on joint angle measurement, which limits its application. Therefore, this paper proposes a new method to calculate the trajectories of anatomical landmarks based on IMC data. The accuracy and reliability of this method were investigated by comparative analysis based on measurement data from 16 volunteers. The results showed that the accuracy of anatomical landmark trajectories was 23.4 to 57.3 mm, about 5.9% to 7.6% of the segment length, the orientation accuracy was about 3.3° to 8.1°, less than 8.6% of the range of motion (ROM), using optical motion capture results as the gold standard. Furthermore, the accuracy of this method is are similar to that of Xsens MVN, a commercial IMC system. The results also show that the algorithm allows for more in-depth motion analysis based on IMC data, and the output format is more versatile.**

***Index Terms*— Inertial motion capture, anatomical landmark, joint coordinate system, kinematic analysis, orientation correction.**

I. Introduction

HUMAN motion measurement is used to obtain information such as body orientation, joint angles, and environmental reaction forces, which are essential foundation in biomechanics, rehabilitation, and human-computer interaction [1]. In healthcare-related applications, motion measurement provides comprehensive joint kinematics and dynamics, thereby enhancing the clinician's understanding of assessment [2], pathology [3], and treatment options [4]. It has the advantage of being objective and quantitative compared to expert judgement. Currently, the gold standard for measuring human motion is optical motion capture (OMC), in which cameras track the trajectories of optical markers attached to anatomical landmarks [5]. Users can use anatomical landmarks to define joint coordinate systems according to various reporting standards as their needs, such as those proposed by the International Society for Biomechanics (ISB) [6]. Although OMC can provide accurate measurements, it has significant limitations, such as expensive equipment, a strict laboratory environment, and trained operators.

Wireless inertial measurement units (IMUs) are increasingly being used to measure human motion [7]. The low cost of the device, its portability to different environments, and its ease of use for any user make it available to medical institutions and families [8], [9]. An IMU consists of an accelerometer, a gyroscope, and a magnetometer. Commercial inertial motion capture (IMC) systems can estimate sensor orientations with respect to a global reference frame through data fusion [10]. However, magnetic disturbances can affect the orientation estimation. Kinematic constraints of the joint are often used to compensate magnetic disturbances. However, most of these studies are based on the assumption of a one degree-of-freedom joint [11], or the joint axes are parallel to the joint coordinate system (JCS) axes [12], and haven't conducted in-vivo verification [11], [12]. In addition, the sensor frame is not aligned with the corresponding body segment frame, and determining the rotation matrix to align them has long been a fundamental challenge for IMC application [13]. Although there are various IMU calibration methods [7], most of the researchers haven't defined the JCS according to the ISB recommendation [6]. The calibration quality, especially for the commonly used functional calibration methods in commercial systems, depends on the quality of the calibration action completion, which will cause calibration errors [7].

Most IMU-based inverse kinematics workflows generate joint angles, such as the OpenSense toolkit in OpenSim [14]. It successfully mitigates drift over long periods of time. However, there was no scaling process for the physiological skeletal

Manuscript received 14 November 2022; revised 29 March 2023; accepted 10 June 2023. Date of publication 14 June 2023; date of current version 21 June 2023. This work was supported in part by the National Key Research and Development Program of China under Grant 2019YFB1312501 and in part by the National Natural Science Foundation of China under Grant 82072042. *(Corresponding author: Suiran Yu.)*

This work involved human subjects or animals in its research. Approval of all ethical and experimental procedures and protocols was granted by the Ethics Committee of the Shanghai Jiao Tong University, under Application No. E2022313I.

Zhengtao Wang, Fei Gao, Zihao Wu, Dongmei Wang, and Suiran Yu are with the School of Mechanical Engineering, Shanghai Jiao Tong University, Shanghai 200240, China (e-mail: sryu@sjtu.edu.cn).

Xin Guo is with the School of Artificial Intelligence and Data Science, Hebei University of Technology, Tianjin 300401, China (e-mail: gxhebut@aliyun.com).

Digital Object Identifier 10.1109/TNSRE.2023.3285924

model. Moreover, the accuracy of IMC is always verified by comparing it with OMC, and joint angle is the common evaluation index [15], [16]. A customer case of Xsens MVN used projected angles in the sagittal plane for validation and the RMSE errors were very low (1.08° to 1.48°) [17]. Another study validated three-dimensional joint angles in Xsens MVN. The Xsens system determined the flexion/extension joint angle most accurately for all joints (1.71 to 3.99°), while for the other two joint axes, the joint angle errors are larger (1.38 to 6.69°) [18]. They believed that the poor correlation in the other two joint axes was most likely due to differences in the JCS definition of the segments used by the Xsens and OMC systems. Due to the different JCS definitions, the effectiveness of the verification remains unknown.

The lack of consistency between different studies and commercial systems makes it difficult to compare and analyze motion measurement results, which will lead to the inability of some motion analysis conclusions to be popularized and used, limiting the development of this field [19]. Without a common convention for defining JCS using IMU data, it is difficult to propose a conventional measurement and analysis protocol. More importantly, many biomechanical analysis methods are based on anatomical landmarks, such as skeletal scaling [20] and the determination of muscle position and direction [21]. The calculation of anatomical landmark trajectories based on inertial measurement data has not received enough attention, and it is a critical problem to be solved.

A possible solution is to output the anatomical landmark trajectories, allowing the user to define JCS according to their needs, and use joint constraints for orientation correction. Picerno et al. [22] developed a calibration procedure for IMC based on the direct identification of palpable anatomical landmarks. The proposed method achieves excellent accuracy of anatomical landmark trajectories, but uses an additional IMU hosted on a caliper-like device. We wanted to develop a more straightforward approach without additional devices.

Since IMC cannot directly measure spatial position and trajectory, the geometric method can obtain anatomical landmark trajectories. First, we need to estimate the anatomical landmark positions in the respective segment frames. A feasible way is to calculate by regression equation with body height or other body dimensions as the input. Although some studies have obtained a large amount of anthropometric data, these studies have focused on how to scale the bone model with marker points to calculate the segment inertia [23] or muscle modeling [5], since most current biomechanical research is based on directly measured anatomical landmark trajectories by OMC. In addition, much attention has been paid to inertial parameters. Ho et al. [24] determined Chinese body segment parameters using a magnetic resonance imaging method. The percentage of segment length from the proximal and distal ends was given. Ma et al. [25] estimated body segment parameters of Korean adults using the three-dimensional (3D) body scan data from the SizeKorea. However, they only focused on the length of each body segment. Body measurements have a high correlation with racial background [26]. Unfortunately, to our knowledge, there is no such database or regression equations of anatomical landmark positions in segment frames of Chinese people. In addition, there is no database of the knee axis of rotation (AoR) direction, which can be used as joint constraints for orientation correction [27].

In summary, the angular accuracy of inertial motion capture has received considerable attention. However, there is a significant difference between anatomical frames calculated from IMC and OMC. Significant challenges remain in comparing the results of different studies. The development of a general convention for defining the anatomical frame for inertial motion capture is essential. Anatomical landmark trajectories are promising because they can be used to define JCS, just like OMC. A fundamental problem to be solved is the regression equations of the anatomical landmark positions and knee AoR direction in segment frames of Chinese people. Therefore, this paper proposed a method to calculate the trajectories of anatomical landmarks based on IMC data. We used OMC data to establish the regression equations. In addition, we calculated the direction of the knee AoR in femoral and tibia frames as a joint constraint to correct the orientation error of IMC, which improved the accuracy of anatomical landmark trajectories. Experimental results showed a good agreement with OMC.

II. Anatomical Landmark Trajectories Calculating Method

The process of anatomical landmark trajectory calculation based on inertial measurement data and verification is shown in Fig. 1., which mainly includes five aspects:

1. Measurement for each subject: we measured the body dimensions, including body height, shank length, knee width, and ankle width, and measured the motion synchronously by IMC and OMC.

2. OMC data processing for each subject: using the anatomical landmark trajectories measured by OMC, we defined the femoral frame, tibia frame, and knee AoR directions in these frames. Then we can get the anatomical landmark positions in femoral and tibia frames.

3. OMC data statistics and analysis for all subjects: we calculated the average knee AoR in femoral and tibia frames and regression equations of anatomical landmark positions in femoral and tibia frames of all subjects.

4. IMC data processing for each subject: using the average knee AoR and the regression equations, we corrected the segment orientations measured by IMC. We calculated the anatomical landmark positions in the femoral and tibia frames. We then calculated the anatomical landmark trajectories for each subject. For verification, it is necessary to unify the global reference frame of IMC and OMC systems. Then we can obtain the trajectory errors.

5. Correlation and agreement analysis for all subjects: Correlation and agreement analysis were conducted for method verification.

Above all, in this section, we first define the joint coordinate system. Second, we introduce the orientation correction method and the anatomical landmark trajectory calculation method. To compare the two systems, we give the process of unifying the reference system. Finally, we describe the experimental protocol.

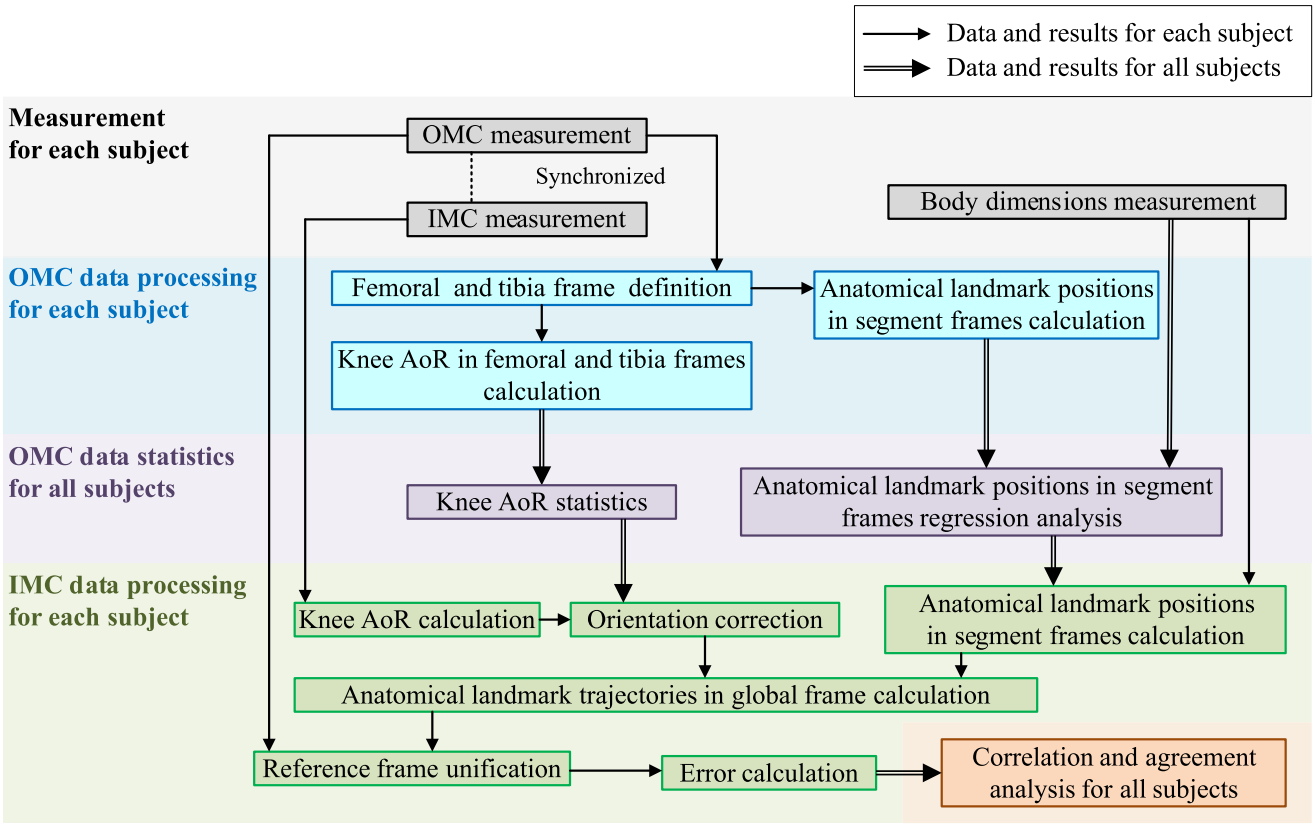

Fig. 1. Method and verification for calculating anatomical landmark trajectories.

A. Joint Coordinate System Definitions

A detailed and efficient understanding of the biomechanics of the lower extremity joint is a prerequisite. This paper discusses the femoral and tibia frames. The pelvis is considered to be fixed. For OMC, the global reference frame $\boldsymbol{G}_{\mathrm{OMC}}$ is defined with the Z-axis pointing up. A cluster of markers which consists of at least three non-collinear markers is attached to each segment of the lower limb. Defining virtual markers in the frame of a cluster of markers allows the tracking of any anatomical landmarks [28]. Four anatomical landmarks are discussed, namely epicondylus femoris medialis (EFM), epicondylus femoris lateralis (EFL), medial malleolus (MM), and lateral malleolus (LM), as shown in Fig. 2.

The hip joint is treated as a ball and socket joint, and the position is calculated using the least square method to fit a sphere, with the center and radius of the sphere optimized to fit the trajectories of the EFM and EFL [29]. The femoral frame of each time frame is defined as described in [6].

To define the tibial frame, the knee AoR must first be determined. The direction of the AoR is determined by the relative rotation between the femoral and tibia frames. The rotation matrix describing the cluster of markers on the tibia ${}^{\mathrm{G}}\boldsymbol{E}^{k}_{\mathrm{T\_cluster}}$ expressed in the femoral frame $\left[{}^{\mathrm{G}}\boldsymbol{E}^{k}_{\mathrm{F}}\right]$ in time frame k is

$$ {}^{\mathrm{F}}\boldsymbol{R}^{k}_{\mathrm{T\_cluster}} = \left[{}^{\mathrm{G}}\boldsymbol{E}^{k}_{\mathrm{F}}\right]^{T} {}^{\mathrm{G}}\boldsymbol{E}^{k}_{\mathrm{T\_cluster}} \tag{1} $$

The rotation of the knee joint in the femoral frame from time frame k to $k+s$ is

$$ {}^{\mathrm{F}}\boldsymbol{R}^{k}_{\mathrm{Knee}} = {}^{\mathrm{F}}\boldsymbol{R}^{k+s}_{\mathrm{T\_cluster}} \left[{}^{\mathrm{F}}\boldsymbol{R}^{k}_{\mathrm{T\_cluster}}\right]^{\mathrm{T}} \tag{2} $$

which can be expressed in form of an axis and angle

$$ {}^{\mathrm{F}}\boldsymbol{R}^{k}_{\mathrm{Knee}} \rightarrow {}^{F}\boldsymbol{V}^{k}_{\mathrm{knee}}, \boldsymbol{A}^{k}_{\mathrm{knee}} \tag{3} $$

Then it can be expressed in the global frame as

$$ {}^{G}\boldsymbol{V}^{k}_{\mathrm{knee}} = {}^{\mathrm{G}}\boldsymbol{E}^{k}_{\mathrm{F}} {}^{F}\boldsymbol{V}^{k}_{\mathrm{knee}} \tag{4} $$

Note that the direction of the rotation axis may be opposite due to the different directions of rotation, since $\boldsymbol{A}^{k}_{\mathrm{knee}}$ is a positive scalar and the direction of ${}^{G}\boldsymbol{V}^{k}_{\mathrm{knee}}$ follows the right-hand rule. For knee flexion, the ${}^{G}\boldsymbol{V}^{k}_{\mathrm{knee}}$ and the Z-axis of the femoral frame are at an obtuse angle, while for knee extension they are at an acute angle. Since we need a rightward knee axis, we can reverse all the knee axes calculated by knee flexion.

Furthermore, there will be moments during the entire sampling when the knee is almost stationary, leading to significant uncertainty in the computed knee AoR, which we want to exclude. The rotation angle during a time step must be greater than a certain threshold, and those ${}^{G}\boldsymbol{V}^{k}_{\mathrm{knee}}$ with too small $\boldsymbol{A}^{k}_{\mathrm{knee}}$ should be removed before further processing. Since the femoral and tibia frames have the same knee AoR expressed in the global reference frame, the knee AoR in time frame k expressed in the femoral frame is

$$ {}^{\mathrm{F}}\boldsymbol{V}^{k}_{\mathrm{knee}} = \left[\boldsymbol{E}^{k}_{\mathrm{F}}\right]^{\mathrm{T}} \left[{}^{G}\boldsymbol{V}^{k}_{\mathrm{knee}}\right] \tag{5} $$

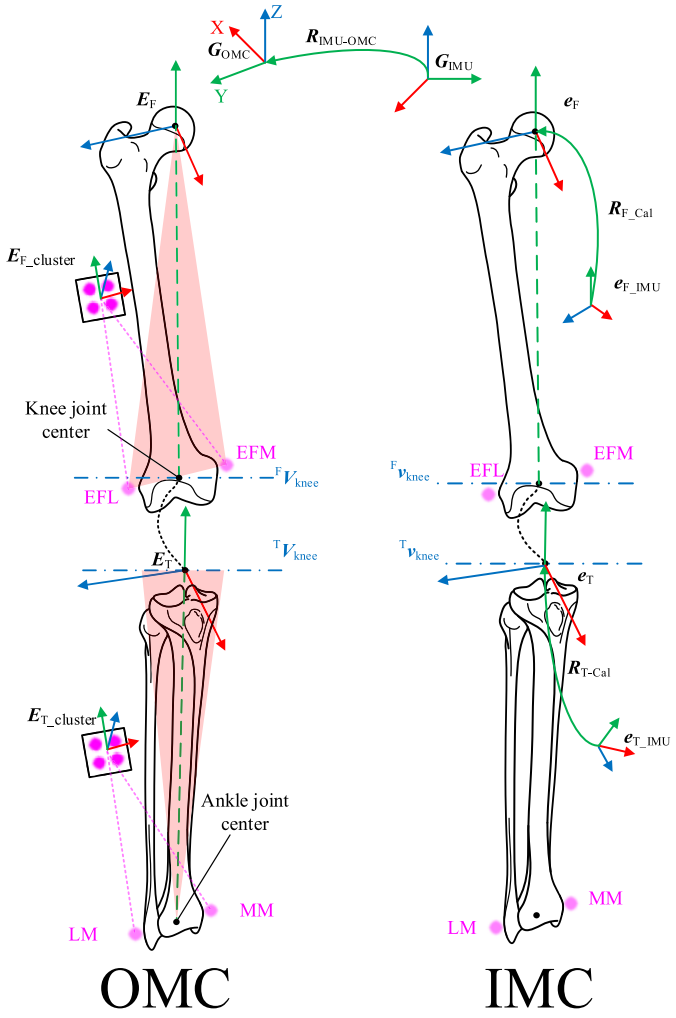

Fig. 2. Illustration of the femoral coordinate system and the tibia/fibula coordinate system.

The weighted average knee AoR is then considered to be the average knee AoR in the femoral frame as

$$ {}^{\mathrm{F}}\boldsymbol{V}_{\mathrm{knee}}^{average} = \frac{\frac{1}{n}\sum \boldsymbol{A}_{\mathrm{knee}}^{k}\,{}^{\mathrm{F}}\boldsymbol{V}_{\mathrm{knee}}^{k}}{\left|\frac{1}{n}\sum \boldsymbol{A}_{\mathrm{knee}}^{k}\,{}^{\mathrm{F}}\boldsymbol{V}_{\mathrm{knee}}^{k}\right|} \tag{6} $$

where n is the number of time frames selected after removing sample points with a small rotation angle during a time step. Then, the tibia frame of each time frame is defined as described in [30].

Note that the Z-axis of the tibia frame is not necessary to be the knee AoR. The knee AoR in time frame k, expressed in the tibia frame, is

$$ {}^{\mathrm{T}}\boldsymbol{V}_{\mathrm{knee}}^{k} = \left[\boldsymbol{E}_{\mathrm{T}}^{k}\right]^{\mathrm{T}}\left[{}^{G}\boldsymbol{V}_{\mathrm{knee}}^{k}\right] \tag{7} $$

The weighted average knee AoR is then considered to be the average knee AoR in the tibia frame as

$$ {}^{\mathrm{T}}\boldsymbol{V}_{\mathrm{knee}}^{average} = \frac{\frac{1}{n}\sum \boldsymbol{A}_{\mathrm{knee}}^{k}\,{}^{\mathrm{T}}\boldsymbol{V}_{\mathrm{knee}}^{k}}{\left|\frac{1}{n}\sum \boldsymbol{A}_{\mathrm{knee}}^{k}\,{}^{\mathrm{T}}\boldsymbol{V}_{\mathrm{knee}}^{k}\right|} \tag{8} $$

Then, we introduce the JCS definitions in IMC. In this paper, we used a commercial motion capture system (FOHEART MAGIC, China, http://foheart.com/en/) in which only the orientation data was used. The orientation of each IMU is expressed relative to the Earth frame. The ideal Earth frame has a z-axis in the opposite direction of gravity, with the y-axis pointing north and the x-axis pointing east. A functional calibration method determines the rotation matrix between the sensor and body frames. The y-axis direction of each body frame is determined by the upright I-pose (the natural standing pose) pointing upward, and the z-axis direction is determined by the Z-pose (the half-squat pose). When converting I-pose to Z-pose, the rotation axis of each sensor is considered to point to the right of the subject as the z-axis of each body frame and reference frame $\boldsymbol{G}_{\mathrm{IMU}}$. Then the IMC system outputs the orientation of each body frame. However, such calibration depends on the quality of the calibration movements, especially in Z-pose, because it is difficult to ensure that each joint rotates only in the sagittal plane. Therefore, we need to use joint constraints to correct the orientation.

B. Orientation Correction and Anatomical Landmark Trajectories Calculation

The average knee AoR can be used as a joint constraint for orientation correction. Because no matter what the measurement system is, they share the same knee AoR. We use $\hat{\boldsymbol{e}}_{\mathrm{T}}^{k}$ to express the tibia frame in time frame k estimated by IMC, which may contain orientation errors due to a poor functional calibration. This error does not affect the orientation of the rotation axis. Therefore, we calculate the rotation matrix of the tibia frame in time frame k with time step s expressed in the reference frame $\boldsymbol{G}_{\mathrm{IMU}}$.

$$ {}^{\mathrm{G}}\boldsymbol{r}_{\mathrm{T}}^{k} = \hat{\boldsymbol{e}}_{\mathrm{T}}^{k+s}\left[\hat{\boldsymbol{e}}_{\mathrm{T}}^{k}\right]^{\mathrm{T}} \tag{9} $$

Using the same method as OMC, we can obtain the average knee AoR in the femoral and tibia frames ${}^{\mathrm{F,T}}\boldsymbol{v}_{\mathrm{knee}}^{average}$. If a poor calibration is performed, the average knee AoR ${}^{\mathrm{F,T}}v_{\mathrm{knee}}^{average}$ will not match the average knee AoR ${}^{\mathrm{F,T}}\boldsymbol{V}_{\mathrm{knee}}^{average}$ measured by OMC. The two angles between these two pairs of AoRs in the femoral and tibia frames are

$$ {}^{\mathrm{F,T}}a = \arccos\left(\frac{{}^{\mathrm{F,T}}\boldsymbol{v}_{\mathrm{knee}}^{average}\,{}^{\mathrm{F,T}}\boldsymbol{V}_{\mathrm{knee}}^{average}}{\left|{}^{\mathrm{F,T}}\boldsymbol{v}_{\mathrm{knee}}^{average}\right|\left|{}^{\mathrm{F,T}}\boldsymbol{V}_{\mathrm{knee}}^{average}\right|}\right) \tag{10} $$

To align these two AoR vectors, we define the rotation axis in the femoral and tibia frames, respectively

$$ {}^{\mathrm{F,T}}\boldsymbol{Axis} = {}^{\mathrm{F,T}}\boldsymbol{v}_{\mathrm{knee}} \times {}^{\mathrm{F,T}}\boldsymbol{V}_{\mathrm{knee}} \tag{11} $$

Then we can express the rotation in the form of rotation matrixes

$$ {}^{\mathrm{F,T}}\boldsymbol{Axis},\ {}^{\mathrm{F,T}}a \rightarrow {}^{\mathrm{F,T}}\boldsymbol{R}_{\mathrm{co}} \tag{12} $$

Finally, we can correct the orientation by right-multiplying the correction matrix

$$ \boldsymbol{e}_{\mathrm{F,T}}^{k} = \hat{\boldsymbol{e}}_{\mathrm{F,T}}^{k}\,{}^{\mathrm{F,T}}\boldsymbol{R}_{\mathrm{co}} \tag{13} $$

which means $\hat{\boldsymbol{e}}_{\mathrm{F,T}}^{k}$ rotates in its own frame by ${}^{\mathrm{F,T}}\boldsymbol{R}_{\mathrm{co}}$.

After the orientation is corrected, the anatomical landmarks trajectories can be calculated. First, the positions of the

anatomical landmarks with respect to the segment frames are estimated using regression equations

$$\boldsymbol{p}_{\text{landmark}} = f\left(d_1, d_2, \ldots, d_n\right) \tag{14}$$

where $d_1, d_2, \ldots, d_{\text{n}}$ are body dimensions such as body height, knee width, ankle width, etc. And corner mark in $\boldsymbol{p}_{\text{landmark}}$ donates which anatomical landmark position is calculated. EFL and EFM trajectories are

$$\boldsymbol{t}^k_{\text{EFL,EFM}} = \left[\boldsymbol{e}^k_{\text{F}}\right]\boldsymbol{p}_{\text{EFL,EFM}} \tag{15}$$

where $\boldsymbol{e}^k_F$ is the orientation matrix of the femoral frames in the time frame k. Then, the knee joint center trajectory is

$$\boldsymbol{t}^k_{\text{knee}} = \left(\boldsymbol{t}^k_{\text{EFL}} + \boldsymbol{t}^k_{\text{EFM}}\right)/2 \tag{16}$$

Then we have the LM and MM trajectories

$$\boldsymbol{t}^k_{\text{LM,MM}} = \left[\hat{\boldsymbol{e}}^k_{\text{T}}\right]\boldsymbol{p}_{\text{LM,MM}} + \boldsymbol{t}^k_{\text{knee}} \tag{17}$$

C. Reference Frame Unification

To compare the anatomical landmark trajectories calculated by the IMC system with those measured by the OMC system, we need to unify the reference frames of the two systems. Since these two systems measure the same motion, motion data is used to unify the reference frames. In this paper, hip flexion is used. Considering the hip joint as the origin, we define the initial frame of each system by the following steps:

Step 1: z_0 and $\boldsymbol{Z}_0$ for IMC and OMC are defined as the unit normal vector of the planes fitted by the knee center trajectories, pointing to the right, respectively.

Step 2: $\boldsymbol{y}_{\text{temp}}$ and $\boldsymbol{Y}_{\text{temp}}$ for IMC and OMC are defined as the y-axis and Y-axis of the femoral frames in the time frame t, respectively.

Step 3: $\boldsymbol{x}_0$ is the unit vector perpendicular to $\boldsymbol{y}_{\text{temp}}$ and z_0, and $\boldsymbol{X}_0$ is the unit vector perpendicular to $\boldsymbol{Y}_{\text{temp}}$ and $\boldsymbol{Z}_0$ for IMC and OMC, respectively.

Step 4: $\boldsymbol{y}_{\text{temp}}$ and $\boldsymbol{Y}_{\text{temp}}$ are not necessarily perpendicular to z_0 and $\boldsymbol{Z}_0$. Therefore $\boldsymbol{y}_0 = z_0 \times \boldsymbol{x}_0$ and $\boldsymbol{Y}_0 = \boldsymbol{Z}_0 \times \boldsymbol{X}_0$ are calculated for IMC and OMC, respectively.

Step 5: The initial frames are defined as $\boldsymbol{G}_{\text{IMU\_init}} = [\boldsymbol{x}_0, \boldsymbol{y}_0, z_0]$ and $\boldsymbol{G}_{\text{OMC\_init}} = [\boldsymbol{X}_0, \boldsymbol{Y}_0, \boldsymbol{Z}_0]$ for OMC and IMC systems respectively.

Then we can calculate the rotation matrix to unify the reference frames

$$\boldsymbol{R}_{\text{IMU\_OMC}} = \boldsymbol{G}_{\text{OMC\_init}}\left[\boldsymbol{G}_{\text{IMC\_init}}\right]^{\text{T}} \tag{18}$$

The anatomical landmark trajectories calculated by the IMC system, expressed in the reference frame of the OMC system, are

$$\boldsymbol{t}^k_{\text{landmark\_OMC}} = \boldsymbol{R}_{\text{IMU\_OMC}}\boldsymbol{t}^k_{\text{landmark}} \tag{19}$$

where $\boldsymbol{t}^k_{\text{landmark}}$ is the anatomical landmark trajectories in time frame k calculated using IMC data with a corner marker denoting the selected anatomical landmark. Considering OMC data as standard, we define the trajectory errors as

$$\boldsymbol{e}^k_{\text{landmark}} = \boldsymbol{t}^k_{\text{landmark\_OMC}} - \boldsymbol{T}^k_{\text{landmark}} \tag{20}$$

where $\boldsymbol{T}^k_{\text{landmark\_OMC}}$ is landmark trajectories in time frame k measured directly by the OMC system.

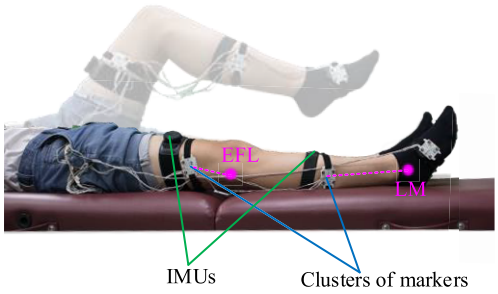

Fig. 3. Placement of IMUs and clusters of markers. The virtual markers are attached to the marker cluster frames. The EFM and MM are on the opposite side of the leg. Subjects were asked to perform a hip flexion.

D. Experimental Protocol

To verify the anatomical landmark trajectory calculation method, 38 healthy subjects (20 males, 176.0 ± 5.2cm, 57.8 ± 11.2kg, 24.5 ± 5.0 years old, and 18 females, 162.4 ± 5.0cm, 53.7 ± 7.1kg, 24.2±3.9 years old) were recruited. The study was exempted from IRB approval by the Ethics Committee of the Shanghai Jiao Tong University. All subjects were informed about the experimental procedure and signed an informed consent form for the experiment. A cluster of active markers (infrared LED) was mounted to each lower limb segment using an elastic band. The 6D motion data of the clusters of markers and 3D virtual anatomical landmark trajectories were recorded at 100Hz by two position sensors with three embedded infrared cameras of the OMC system (Optotrak Certus, NDI, Canada). Among these subjects, 16 healthy subjects (6 males, 174.83 ± 4.2cm height, 66.4 ± 11.4kg weight, 24.7 ± 2.4 years old, and 10 females, 161.5 ± 4.62cm height, 54.6 ± 8.7kg, 24.4 ± 1.3 years old) were also mounted with IMUs (FOHEART MAGIC, China).

An embedded fusion algorithm was used to estimate the orientation of the sensor relative to the Earth frame. We didn't try other fusion algorithms because our main focus was to compute anatomical landmark trajectories. The orientation accuracy of the IMUs is $\leq 0.5°$ RMS in roll/pitch and $\leq 2°$ RMS in yaw [31]. The orientation of each body segment was recorded at 100Hz. Data from the two systems were manually synchronized using peak values. The in-vivo study was conducted in a typical reinforced concrete building. There was no large electrical equipment around, and no strong magnetic distortions. We performed sensor calibration before the experiment, and ensured that the software did not display magnetic distortions during calibration and recording. The IMUs and clusters of markers placement are shown in Fig. 3.

This work is supported by the National Key Research and Development Program of China (No. 2019YFB1312501). The program aims to develop personalized rehabilitation plans for spinal cord injury patients and determine the motion parameters of rehabilitation robots based on objective motor function assessment. The current gold standard for measuring motor function after SCI is the American Spinal Injury Association (ASIA) Impairment Scale (AIS). Therefore, we designed the experimental protocol according to the ASIA Motor Exam Guide [32]. This paper focuses on the hip and knee joints, and we have selected movements that included both hip flexion and knee flexion. Each subject was asked to lie supine on

a wooden bed to simulate a clinical examination scenario, avoid pelvic movement, and perform hip flexion trials. The instructions were: "Please lift and lower your upper leg. Try not to drag your foot on the exam bed." The motions are shown in Fig. 3.

In addition, to our knowledge, few studies have used anatomical landmark trajectories as an evaluation index. We used another IMC system (Xsens MVN, version 2021.2.0, Netherlands) for comparison. The same OMC system (Optotrak Certus, NDI, Canada) was used and recorded at 100Hz. Two healthy male subjects (29 and 27 years old, 171 and 174 cm, 58 and 63kg) were recruited. IMU sensors (Xsens Link) and the cluster of active markers for optical motion capture were attached to each lower limb segment using elastic bands. Before recording, the subject was asked to perform MVN calibration. The subject first performed an N-pose, standing in an upright and natural position, with the feet parallel and pointing forward with about one foot-width distance in between the feet. We asked the subject to hold the N-Pose for a few seconds. Then, with the indication from the software, the subject was asked to walk straight forward and turn back, then perform the N-pose again (the latest software asks the subject to walk around). After calibration, we asked the subject to lie supine on a wooden examination bed and perform hip flexion and record IMC and OMC data. After recording, we used Reprocess HD in Xsens MVN. We also asked Subject 1 to perform a non-standard calibration. We asked him to flex the knee joint while performing N-Pose. The walking calibration was performed normally. IMC and OMC data were manually synchronized using peak values.

The positions of the anatomical landmarks with respect to the segment frames are estimated using regression equations. For comparison, we compare the results of our OMC measurements with the scaling result of Xsens MVN (version 2021.2.0). Instead of using the sensors to measure actual motion, we keep the sensors still on the table throughout the process. Before each recording, we entered the body height ranging from 150cm to 190cm with a 10cm increments. Other body segment dimensions were automatically adjusted by the software. We then performed the MVN calibration. Since the sensors were not moved, the MVN model was in an N-pose. We recorded the static data for several seconds. Finally, we output the data in .c3d and .xls format. The landmark positions are read from the .c3d file. The joint positions are read from the .xls file. We defined the femoral and tibia frames as mentioned in our paper. Note that we cannot get a knee AoR from static data, so we adopted the Xsens MVN tibia z-axis as the knee AoR instead. According to the MVN user manual, the tibia z-axis is defined as the line from medial to lateral pointing to the right. We then calculated the landmark positions in segment frames for different heights.

All data processing was done in MATLAB 2022a, the data and codes are available at [33].

III. Results

This section presents the regression results of anatomical landmark positions in the segment frame, the knee AoR direction, and trajectory errors.

A. Anatomical Landmark Positions in Segment Frames

For OMC data, the femoral and tibia frames were calculated according to the definition proposed in 2.1. Several regression equations were used to calculate the anatomical landmark positions in the segment frames. A k-fold cross validation approach was used. The data were divided into K parts. $K-1$ parts were used for linear regression and one part for testing and we got K groups of parameters. We calculated the mean value of K groups of parameters and gave the mean test error $\pm$ standard deviation (SD) to evaluate the effectiveness.

First, the linear regression using the least square method of anatomical landmark positions in segment frames with respect to body height h is investigated. Regression equations $p = b_0 + b_1 h$ of anatomical landmark positions p and height h are shown in Tab. I. and Fig. 4. Dimensions in y direction show good correlation with p-value < 0.05 and the coefficient of determination $R^2 = 0.240$ to 0.825, while other directions show lower or even no correlation (p-value > 0.05). The SD of the test error is greater than 10mm in the y-direction, while it is less than 10mm in other directions. It shows that in this age group, the difference in bone dimension is mainly in the y-direction and has more significant individual differences.

Second, we introduced shank length as an independent variable for regression analysis. It can be measured laterally (distance between EFL and LM) as s_{L} or medially (distance between EFL and LM) as s_{L}. The regression equations $p = b_0 + b_1 h + b_2 s_{\mathrm{L}}$ and $p = b_0 + b_1 h + b_2 s_{\mathrm{M}}$ are shown in Tab. I. The R^2 of y-directions of MM and ML increased to 0.872 to 0.995, while there is no significant increase for the y-directions of EFM and EFL.

Third, we investigated the relationship between knee width k (distance between EFM and EFL) and EFM and EFL positions in the z-direction. The regression equation $p = b_0 + b_1\ k$ has $\mathrm{R}^2 = 1$, as shown in Tab. I.

Finally, we used h and ankle width a (distance between MM and LM) as independent variables, the regression equation $p = b_0 + b_1 h + b_2 a$ for MM and ML positions in the x- and z-directions. The reduction of the test error is limited, from 2.5 to 7.1mm down to 2.0 to 7.1mm, as shown in Tab. I.

We also compare the Xsens MVN scaling results with our OMC measurement results and there are significant errors, as shown in Tab. II and Fig. 4. Since it's a European company, we believe that the scaling parameters are for European people. We recommend that the scaling of inertial motion capture can take gender and race into account.

B. Knee AoR Orientation

We calculated the directions of the knee AoRs in the femoral and tibial frames of each subject using the OMC data. Then, we averaged all the knee AoRs and calculated the SD of their projection angles in the transverse and frontal planes. The results of the OMC data calculation are shown in Fig. 5., and the values are shown in Tab. III.

C. Anatomical Landmark Trajectories

First, we calculated the anatomical landmark positions in the segment frames. We used the regression equation with the smallest SD from Tab. I to calculate each landmark position in

TABLE I
REGRESSION EQUATIONS OF ANATOMICAL LANDMARK POSITIONS IN SEGMENT FRAMES (UNIT: mm)

Gender	Equation	Position	b_0	b_1	b_2	R^2	p	Mean error ± SD
Male	$p = b_0+b_1h$	EFM Y	-11.949	-0.232	0.000	0.240	0.042	-0.0±23.3
		EFM Z	-51.859	0.001	0.000	0.007	0.811	-0.1±4.6
		EFL Y	-3.102	-0.238	0.000	0.238	0.043	0.1±24.0
		EFL Z	51.859	-0.001	0.000	0.007	0.811	0.1±4.6
		MM X	-65.268	0.045	0.000	0.136	0.179	0.0±7.1
		MM Y	156.409	-0.312	0.000	0.603	0.000	0.2±15.0
		MMZ	-37.062	0.004	0.000	0.018	0.686	0.0±4.4
		LM X	65.268	-0.045	0.000	0.136	0.179	-0.0±7.1
		LM Y	125.652	-0.300	0.000	0.521	0.001	0.3±17.3
		LMZ	37.062	-0.004	0.000	0.018	0.686	-0.0±4.4
	$p = b_0+b_1h+b_2s_L$	MM Y	62.698	-0.084	-0.766	0.900	0.000	-0.4±7.9
		ML Y	2.830	-0.002	-0.999	0.994	0.000	0.1±2.1
	$p = b_0+b_1h+b_2s_M$	MM Y	-3.641	-0.001	-0.983	0.994	0.000	-0.1±1.8
		ML Y	-31.098	0.005	-0.962	0.872	0.000	0.4±8.7
	$p = b_0+b_1k$	EFM Z	-0.052	-0.499	0.000	1.000	0.000	-0.0±0.0
		EFL Z	0.052	0.499	0.000	1.000	0.000	0.0±0.0
	$p = b_0+b_1h+b_2a$	MM X	-67.707	0.053	-0.172	0.144	0.348	0.1±7.1
		ML X	-44.878	0.031	-0.582	0.279	0.092	-0.0±3.8
		MM Z	67.707	-0.053	0.172	0.144	0.348	-0.1±7.1
		ML Z	44.878	-0.031	0.582	0.279	0.092	0.0±3.8
Female	$p = b_0+b_1h$	EFM Y	568.010	-0.584	0.000	0.821	0.000	-0.0±14.7
		EFM Z	49.089	-0.060	0.000	0.395	0.012	0.0±4.1
		EFL Y	494.029	-0.539	0.000	0.825	0.000	-0.0±13.0
		EFL Z	-49.089	0.060	0.000	0.395	0.012	-0.0±4.1
		MM X	27.017	-0.011	0.000	0.027	0.584	-0.1±4.3
		MM Y	28.396	-0.238	0.000	0.288	0.041	0.7±24.5
		MMZ	13.842	-0.026	0.000	0.237	0.062	0.0±2.5
		LM X	-27.017	0.011	0.000	0.027	0.584	0.1±4.3
		LM Y	87.397	-0.281	0.000	0.337	0.023	0.6±24.4
		LMZ	-13.842	0.026	0.000	0.237	0.062	-0.0±2.5
	$p = b_0+b_1h+b_2s_L$	MM Y	-66.412	0.019	-0.874	0.887	0.000	0.6±9.6
		ML Y	-35.334	0.024	-1.007	0.995	0.000	-0.0±1.9
	$p = b_0+b_1h+b_2s_M$	MM Y	35.417	-0.026	-0.980	0.995	0.000	0.0±2.0
		ML Y	94.747	-0.074	-0.955	0.896	0.000	-0.1±9.0
	$p = b_0+b_1k$	EFM Z	-0.152	-0.498	0.000	1.000	0.000	-0.0±0.1
		EFL Z	0.152	0.498	0.000	1.000	0.000	0.0±0.1
	$p = b_0+b_1h+b_2a$	MM X	32.367	-0.029	0.409	0.324	0.108	0.0±4.0
		ML X	9.613	-0.011	-0.313	0.632	0.002	0.0±2.0
		MM Z	-32.367	0.029	-0.409	0.324	0.108	-0.0±4.0
		ML Z	-9.613	0.011	0.313	0.632	0.002	-0.0±2.0
All	$p = b_0+b_1h$	EFM Y	152.541	-0.327	0.000	0.654	0.000	0.1±21.9
		EFM Z	-17.807	-0.019	0.000	0.124	0.045	-0.3±4.3
		EFL Y	150.981	-0.326	0.000	0.669	0.000	0.1±21.2
		EFL Z	17.807	0.019	0.000	0.124	0.045	0.3±4.3
		MM X	-37.700	0.029	0.000	0.180	0.022	-0.3±5.8
		MM Y	60.655	-0.258	0.000	0.658	0.000	-0.2±16.3
		MMZ	-4.096	-0.015	0.000	0.142	0.041	-0.1±3.4
		LM X	37.700	-0.029	0.000	0.180	0.022	0.3±5.8
		LM Y	54.805	-0.260	0.000	0.628	0.000	-0.4±17.4
		LMZ	4.096	0.015	0.000	0.142	0.041	0.1±3.4
	$p = b_0+b_1h+b_2s_L$	MM Y	17.014	-0.042	-0.834	0.928	0.000	0.1±8.3
		ML Y	-1.785	0.002	-1.001	0.996	0.000	0.0±2.1
	$p = b_0+b_1h+b_2s_M$	MM Y	1.254	-0.005	-0.977	0.996	0.000	-0.0±2.0
		ML Y	-2.550	-0.017	-0.940	0.921	0.000	-0.5±8.7
	$p = b_0+b_1k$	EFM Z	-0.093	-0.499	0.000	1.000	0.000	-0.0±0.1
		EFL Z	0.093	0.499	0.000	1.000	0.000	0.0±0.1
	$p = b_0+b_1h+b_2a$	MM X	-29.259	0.014	0.257	0.217	0.029	-0.3±5.7
		ML X	-17.006	0.008	-0.394	0.392	0.001	-0.1±2.9
		MM Z	29.259	-0.014	-0.257	0.217	0.029	0.3±5.7
		ML Z	17.006	-0.008	0.394	0.392	0.001	0.1±2.9

where h is the body height, s_L is the distance between ML and EFL, s_M is the distance between MM and EFM, k is the knee width, and a is the ankle width.

the segment frame. Fig. 6. shows the results of the anatomical landmark trajectories calculated using IMC data compared with the OMC data of one subject. In Fig. 6. (a) and (b), the hip joint is moved to the origin. The trajectories calculated from IMC data are green dots, and the OMC data are blue. The error vectors are shown in pink. Only a subset of the data points are plotted for illustration. 3D skeletal models in three selected time frames are also drawn to better understand the motion. In Fig. 6. (a) represents the result without correction, and we can see that LM and MM are obviously biased

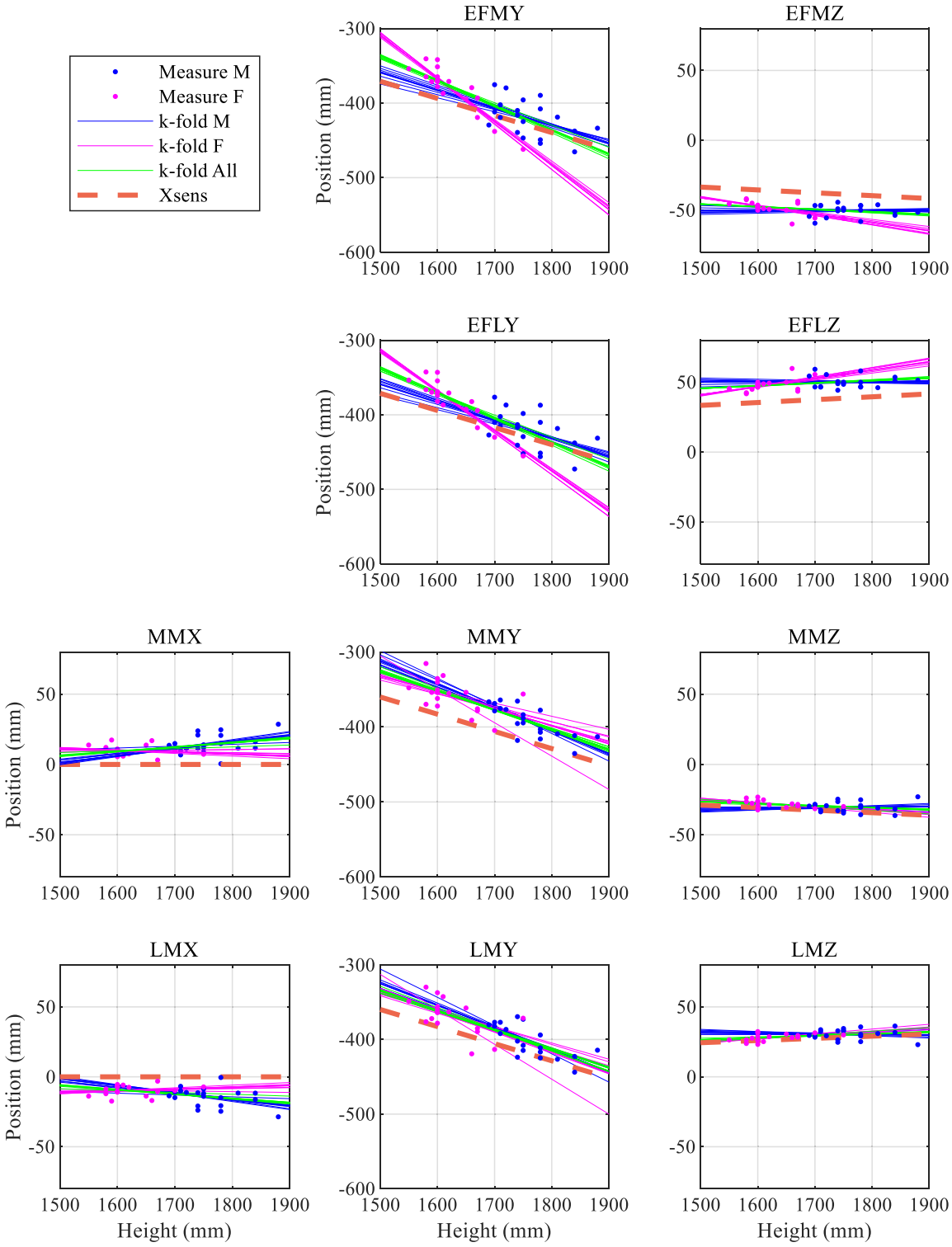

Fig. 4. Regression results of atomical landmark positions in segment frames, where M is male and F is female.

to one side (negative y-axis direction), which indicates that the orientation of the knee AoR is biased. It can be better illustrated in In Fig. 6. (c), as the green points (y direction) are above the $x = y$ line. To verify the effect of the orientation correction, we give the orientation correction results using the average knee AoR. The trajectory errors are reduced, as shown in In Fig. 6. (b) and (d).

The root mean square (RMS) errors of all 16 subjects are shown in Tab. IV. For the results without orientation correction, the errors of MM and ML are relatively large. With orientation correction using the knee AoR, the errors of MM and ML are reduced. Although there are significant differences in the direction of the knee AoR for each person, the correction using the average AoR obtained from the OMC

TABLE II
XSENS MVN SCALING ERRORS COMPARED TO OMC MEASUREMENT RESULTS (UNIT: mm)

Gender	Position	X	Y	Z
Male	REFM		-9.9±21.5	11.4±4.3
	REFL		-9.0±22.1	-11.4±4.3
	RMM	-14.3±6.6	-27.2±13.8	-3.1±3.9
	RLM	14.3±6.6	-17.3±15.4	-2.0±3.8
Female	REFM		-18.6±22.2	12.3±4.2
	REFL		-18.8±19.6	-12.3±4.2
	RMM	-9.6±4.0	-30.2±18.4	-3.1±2.3
	RLM	9.6±4.0	-19.9±19.4	-1.7±2.3
All	REFM	0.0±0.0	-14.0±22.0	11.9±4.2
	REFL	0.0±0.0	-13.7±21.3	-11.9±4.2
	RMM	-12.1±6.0	-28.6±16.0	-3.1±3.2
	RLM	12.1±6.0	-18.5±17.2	-1.9±3.2

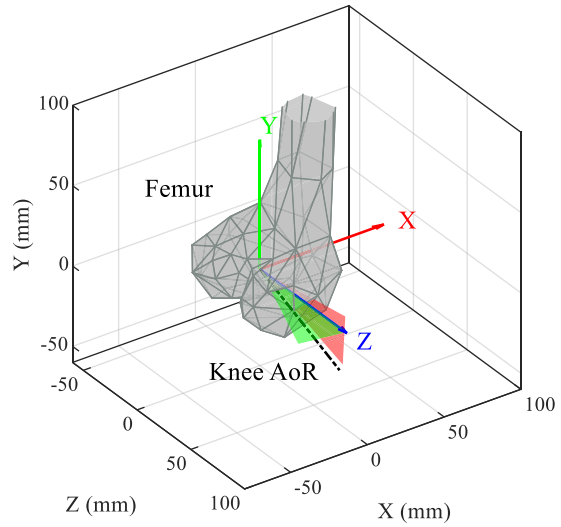

(a) Average knee AoR in femoral frame calculated from OMC data

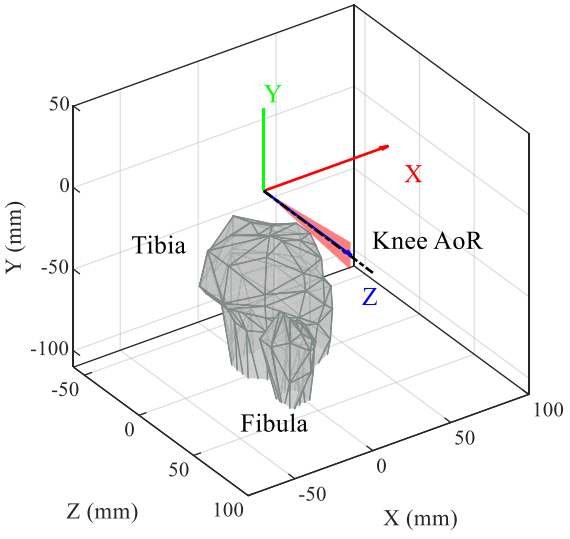

(b)Average knee AoR in tibia frame calculated from OMC data

Fig. 5. Average knee AoR in femoral and tibia frames with ± SD bounds projected in transverse (green) and frontal (red) planes.

data can still reduce the errors as a whole (23.4±7.4mm to 57.3±27.5mm), about 5.9% to 7.6% of the segment length. Using individual AoR for correction can further reduce the errors (28.0±9.8 mm to 50.0±21.6mm). Note that RMS errors without correction are sometimes lower than those with average AoR correction, and RMS errors with average AoR correction are sometimes lower than those with individual AoR correction, which is strange. This could be because the placement of marker clusters and IMUs is different, and the effect of soft tissue deformation on them is also different. As a result, the estimated knee AoRs may not be the same, causing a slight increase in the errors of EFM and EFL, while still reducing the errors of MM and LM.

The correlation between the two systems is assessed using the Pearson correlation coefficients r. The correlation thresholds are defined as poor (< 0.4), modest (0.40 to 0.74), and excellent (≥ 0.75) [34]. In addition, a high correlation between two systems does not necessarily mean that they have a good absolute agreement. Therefore, in this study the intraclass correlation coefficient (ICC) is used to evaluate the absolute agreement between the two systems. The ICC is interpreted as poor (< 0.4), fair (0.4 to 0.59), good (0.6 to 0.74), and excellent (≥ 0.75) [35].

The four anatomical landmark trajectories calculated using IMC data (regression equations and average AoR correction) are discussed in three directions. The correlation between the two systems is calculated and averaged for each subject. For each anatomical landmark, $r = 0.999$ in the x direction, $r = 0.723$ to 0.824 in the y direction, and $r = 0.960$ to 0.999 in the z direction. The ICCs are 0.999 in the x direction, 0.773 in the y direction, and 0.981 in the z direction. This indicates that our method can achieve excellent agreement results with OMC for the movement in the sagittal plane and good agreement results in other anatomical planes.

We investigate the influence of anatomical landmark positions in segment frames by analyzing the correlation between trajectory results calculated by regression equations and OMC data. The correlation between these two methods reached $r > 0.97$ for all subjects. It shows that our regression equations have a good agreement with OMC results.

In addition, we investigate the influence of individual knee AoR orientation differences on the orientation correction by analyzing the correlation between the results obtained by the average AoR correction and the individual AoR correction. It shows that the r for EFM and EFL is 0.97 and for MM and LM is 0.93, which shows an excellent correlation.

Furthermore, we calculated the orientation errors by dividing the rotation matrix of the IMC and OMC data and converting it into Euler angles (Z-Y-X), as shown in Tab. V. The results showed that our correction method could reduce the orientation errors to 3.3° to 8.1°. Considering the range of motion (ROM) from the N-pose to the experimental movements of the femoral and tibia frames, the average ROM was 157° and 87°, respectively. Orientation errors are less than 8.6% ROM and are acceptable.

Finally, data from two subjects recorded by Xsens MVN and OMC were also processed. Xsens MVN exported data in C3D format and was processed only to unify the reference frame with OMC. The RMS errors of the anatomical landmark trajectories are shown in Tab. VI. For subject 1, we give

TABLE III
KNEE AOR UNIT VECTORS AND PROJECTION ANGLES

	Femoral frame		Tibia frame	
	Male	Female	Male	Female
Mean knee AoR	[-0.121, -0.169, 0.978]	[-0.172, 0.057, 0.983]	[0, -0.006, 0.999]	[0, 0.002, 0.999]
Angle in frontal plane (YZ)	-9.69° ± 6.67°	-3.42° ± 6.73°	-0.35° ± 6.67°	0.11° ± 2.47°
Angle transverse plane (XZ)	-6.97° ± 11.28°	-9.94° ± 7.18°	—	—

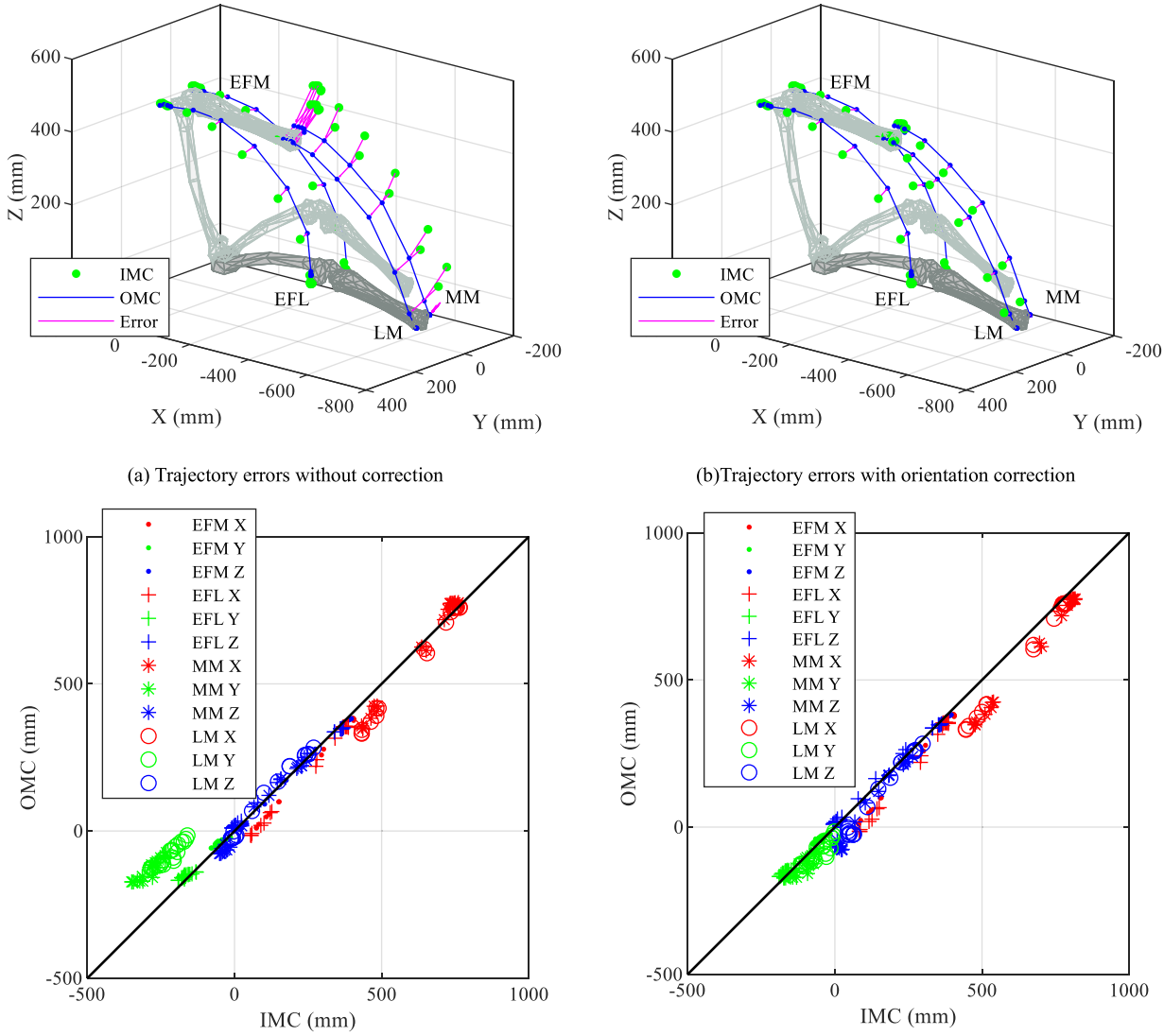

(a) Trajectory errors without correction

(b)Trajectory errors with orientation correction

(c) Comparison of coordinate values in three directions without correction

(d) Comparison of coordinate values in three directions with orientation correction

Fig. 6. Anatomical landmark trajectories calculated from IMC data compared to OMC data. Only a subset of data points are shown for illustration.

results of 2 calibrations, the first calibration is non-standard as described in the experimental protocol. And it shows very large errors. This indicates that the completion quality of the calibration action affects the measurement accuracy. The other three experiments show lager errors than our method. A possible reason is that the regression equations of anatomical landmark positions in segment frames adopted by Xsens MVN are unsuitable for Chinese. We also calculated the orientation errors as shown in Tab. VII. Note that the large ROM from N-pose to experimental movements, and the orientation errors are less than 8.8% ROM on average, similar to our that of our method.

IV. DISCUSSION

We have established regression equations of Chinese anatomical landmark positions in femoral and tibia frames, which is consistent with the recommendation of the ISB. This is groundbreaking and provides a complete set of procedures for future research to establish more comprehensive regression

TABLE IV
RMS ERRORS OF LANDMARK TRAJECTORIES (UNIT: mm)

Position calculation method	Orientation correction method		RMS errors (mean ± SD)			
			EFM	EFL	MM	ML
Regression equations	Without correction	Male	26.5±6.8	25.8±7.1	115.1±66.7	117.8±67.0
		Female	34.4±8.6	33.4±10.0	82.1±47.8	81.4±48.1
	Average AoR correction	Male	26.5±6.3	23.4±7.4	53.3±10.5	55.1±13.0
		Female	32.6±9.1	31.9±9.6	57.3±27.5	56.0±27.4
	Individual AoR correction	Male	29.4±12.1	28.0±9.8	49.6±14.6	47.6±13.7
		Female	29.8±12.3	29.6±12.1	48.5±24.2	50.0±21.6
Directly obtained by individual OMC data	Without correction	Male	21.8±9.0	21.4±7.2	113.6±67.1	114.2±68.7
		Female	31.0±9.9	30.2±10.8	80.2±42.7	79.9±45.7
	Average AoR correction	Male	22.8±4.9	18.6±7.1	50.5±12.2	52.3±13.3
		Female	29.1±9.8	28.4±10.6	54.6±24.2	54.1±24.9
	Individual AoR correction	Male	26.1±11.6	24.4±8.6	42.2±15.2	43.1±14.1
		Female	26.1±12.3	25.7±13.0	45.0±17.5	47.0±18.2

TABLE V
RMS ERRORS OF ORIENTATION FOR ALL SUBJECTS (MEAN ± SD)

Orientation correction method	Orientation errors of femur frame			Orientation errors of tibia frame		
	Z	Y	X	Z	Y	X
Without correction	3.7±2.7°	3.5±2.6°	9.2±7.6°	18.8±9.9°	4.0±1.9°	8.9±5.7°
Average AoR correction	4.2±2.5°	3.4±0.8°	8.1±3.4°	6.8±3.1°	3.3±0.7°	7.6±2.7°

TABLE VI
RMS ERRORS OF ANATOMICAL LANDMARK TRAJECTORIES USING XSENS MVN (UNIT: mm)

Trails	EFM	EFL	MM	ML
Subject 1, calibration 1	46.5	62.4	248.8	267.7
Subject 1, calibration 2	43.9	61.4	126.7	145.1
Subject 2, calibration 1	78.0	56.5	136.1	119.2
Subject 2, calibration 1	86.3	69.5	145.3	133.2

equations, which is the basis for calculating landmark trajectories using IMC data.

The regression equations using the body height as the independent variable can calculate the anatomical landmark positions, but there is a large SD in the y-direction. The shank length can be introduced to improve the accuracy of the regression equations, but only the error of the MM and ML positions in the y direction can be reduced. The knee width can be used to accurately obtain the EFM and EFL positions in the z-direction. However, the measurement of the ankle joint width does not help to significantly improve the positional accuracy of the MM and ML in the x and z directions. Users can select different regression equations for calculation as needed.

Orientation errors have a large influence on the calculation result of the anatomical landmark trajectories. For IMU orientation estimation, we used a commercial inertial motion capture system with an embedded fusion algorithm. We didn't try other sensor fusion algorithms. We assume that the system has an error of 2° [31]. And we conducted the in-vivo study on a wooden bed, trying to avoid magnetic disturbances. Another source of orientation error is the sensor-to-segment calibration error, since we used functional calibration methods in the commercial system which depends on the quality of the calibration action completion. We tried to correct the orientation error using joint constraints. Unlike other approaches, we didn't consider the joint axis as one of the segment frames axes [12]. Using the OMC data, we get the statistical average knee axis of Chinese young people. It is obvious that the knee AoR in the femoral frame is not orthogonal to any axis of the femoral frame, while the knee AoR in the tibia frame is almost coincides with the z-axis of the tibia frame. In addition, the SD of the knee AoR projection angles cannot be ignored. We compared the difference and correlation between the results using average AoR and individual AoR for orientation correction. Individual differences in AoR orientation have a negative but not obvious effect on the correction. We didn't consider the knee joint as a hinge joint and correct the orientation error using individual correction rotation matrices for each time frame [11]. We calculate the average knee AoR direction of the entire measurement, and correct the orientation error using the same correction rotation matrix for each time frame, and the joint angles are three-dimensional. This approach would compensate the magnetic disturbances and the calibration error at the same time.

This paper aims to estimate the anatomical landmark positions in the segment frame and apply the orientation of the segments to all position vectors to obtain trajectories. We haven't discussed the spatial motion of the pelvis. However, our approach can be combined with other gait measurement methods. Typically, IMU for gait measurement suffers from drift. One of the known approaches is to reset the velocity to zero when the foot hits the ground, namely zero velocity update (ZUPT) [36]. In this method, if the length vector of each segment is known, the drift error can be reduced by taking the orientation as input and calculating the

TABLE VII
RMS ERRORS OF ORIENTATION USING XSENS MVN

Orientation correction method	Orientation errors of femoral frame			Orientation errors of tibia frame		
	Z	Y	X	Z	Y	X
Subject 1, calibration 1	4.5°	17.0°	12.1°	36.6°	5.7°	3.1°
Subject 1, calibration 2	4.2°	5.7°	5.9°	17.2°	7.9°	2.1°
Subject 2, calibration 1	11.1°	9.8°	13.8°	5.8°	6.4°	12.7°
Subject 2, calibration 1	12.2°	13.6°	14.6°	3.1°	9.6°	12.9°

step length vector through the kinematic chains. Our method provides an easy way to obtain the segment length, as it is not easy for the untrained person to measure the joint center.

To our knowledge, few studies have considered the trajectories accuracy of anatomical landmarks. Therefore, we also calculated the orientation error, and the results are comparable with those presented studies using the functional calibration method. Note that the ROM of our study are larger than that of gait measurement. Favre et al. [15] achieved moderate joint angle accuracy (4.0 to 8.1°). Liu et al. [13] proposed a calibration method that effectively suppresses the shaking disturbances, and the orientation errors are 5.8 ± 3.2°. The Xsens MVN native protocols most accurately determined the flexion/extension joint angle, while the joint angle measurements associated with the other two joint axes had lower accuracy (1.38 to 6.69°) [18].

In summary, our method achieves ideal results. Our regression equations for the anatomical landmark positions in the segment frame calculation are in good agreement with the OMC measurement results. Note that the orientation accuracy of our IMU is lower than that of the Xsens MVN. The orientation correction method using the average AoR makes our trajectory error smaller than the Xsens MVN native protocols, and has similar joint angle errors to that of Xsens MVN when ROM is taken into account. However, the individual differences in knee AoR should be considered in future research, as the use of average AoR and individual AoR does not achieve the best correlation. This may be due to other confounding factors not accounted for in this study. For example, the placement of the marker clusters and the IMUs are different, and the effect of soft tissue deformation on them is also different. As a result, the estimated knee AoRs may not be the same, which is why the error of the two anatomical landmarks of the femoral frame slightly increases after orientation correction.

V. CONCLUSION

This paper provided a new output format for inertial motion capture, allowing users to define joint coordinate systems according to their needs and compare them more effectively with optical motion capture systems. For the first time, we proposed regression equations of Chinese anatomical landmark positions in a segment frame that conforms to the ISB standard. We also proposed an orientation correction method using joint constraints, which improves the accuracy of anatomical landmark trajectories. Experimental results showed a good agreement with optical motion capture as the gold standard and the accuracy of this method is are similar to that of Xsens MVN. Although there is still a gap in accuracy compared with optical motion capture, this method enables human motion measurement to be used in more scenarios.

REFERENCES

[1] T. B. Moeslund, A. Hilton, and V. Krüger, "A survey of advances in vision-based human motion capture and analysis," *Comput. Vis. Image Understand.*, vol. 104, nos. 2–3, pp. 90–126, Nov. 2006.

[2] J. C. van den Noort, V. A. Scholtes, and J. Harlaar, "Evaluation of clinical spasticity assessment in cerebral palsy using inertial sensors," *Gait Posture*, vol. 30, no. 2, pp. 43–138, Aug. 2009.

[3] G. L. Hatfield, C. L. Hubley-Kozey, J. L. A. Wilson, and M. J. Dunbar, "The effect of total knee arthroplasty on knee joint kinematics and kinetics during gait," *J Arthroplasty*, vol. 26, no. 2, pp. 309–318, Feb. 2011.

[4] C. Mittag, R. Leiss, K. Lorenz, and T. Seel, "Development of a home-based wrist range-of-motion training system for children with cerebral palsy," *At Automatisierungstechnik*, vol. 68, no. 11, pp. 967–977, Nov. 2020.

[5] A. Rajagopal, C. L. Dembia, M. S. DeMers, D. D. Delp, J. L. Hicks, and S. L. Delp, "Full-body musculoskeletal model for muscle-driven simulation of human gait," *IEEE Trans. Biomed. Eng.*, vol. 63, no. 10, pp. 2068–2079, Oct. 2016.

[6] G. Wu et al., "ISB recommendation on definitions of joint coordinate system of various joints for the reporting of human joint motion—Part I: Ankle, hip, and spine," *J. Biomech.*, vol. 35, no. 4, pp. 543–548, Apr. 2002.

[7] R. V. Vitali and N. C. Perkins, "Determining anatomical frames via inertial motion capture: A survey of methods," *J. Biomech.*, vol. 106, Jun. 2020, Art. no. 109832.

[8] P. Daponte, L. De Vito, M. Riccio, and C. Sementa, "Design and validation of a motion-tracking system for ROM measurements in home rehabilitation," *Measurement*, vol. 55, pp. 82–96, Sep. 2014.

[9] J. Kim, N. Colabianchi, J. Wensman, and D. H. Gates, "Wearable sensors quantify mobility in people with lower limb amputation during daily life," *IEEE Trans. Neural Syst. Rehabil. Eng.*, vol. 28, no. 6, pp. 1282–1291, Jun. 2020.

[10] G. Ligorio and A. M. Sabatini, "A novel Kalman filter for human motion tracking with an inertial-based dynamic inclinometer," *IEEE Trans. Biomed. Eng.*, vol. 62, no. 8, pp. 2033–2043, Aug. 2015.

[11] D. Laidig, T. Schauer, and T. Seel, "Exploiting kinematic constraints to compensate magnetic disturbances when calculating joint angles of approximate Hinge joints from orientation estimates of inertial sensors," in *Proc. Int. Conf. Rehabil. Robot. (ICORR)*, Jul. 2017, pp. 971–976.

[12] R. Vitali et al., "Method for estimating three-dimensional knee rotations using two inertial measurement units: Validation with a coordinate measurement machine," *Sensors*, vol. 17, no. 9, p. 1970, Aug. 2017.

[13] Y.-T. Liu, Y.-A. Zhang, and M. Zeng, "Sensor to segment calibration for magnetic and inertial sensor based motion capture systems," *Measurement*, vol. 142, no. 8, pp. 1–9, 2019.

[14] M. Al Borno et al., "OpenSense: An open-source toolbox for inertial-measurement-unit-based measurement of lower extremity kinematics over long durations," *J. NeuroEng. Rehabil.*, vol. 19, no. 1, p. 22, Feb. 2022.

[15] J. Favre, R. Aissaoui, B. M. Jolles, J. A. de Guise, and K. Aminian, "Functional calibration procedure for 3D knee joint angle description using inertial sensors," *J. Biomech.*, vol. 42, no. 14, pp. 2330–2335, Oct. 2009.

[16] T. Seel, J. Raisch, and T. Schauer, "IMU-based joint angle measurement for gait analysis," *Sensors*, vol. 14, no. 4, pp. 6891–6909, Apr. 2014.

[17] I. Scirlet and M. Kraft. *Development and Validation of an Inertial Sensor Based Human Model With Integrated Compensation of Errors*. Accessed: Mar. 17, 2023. [Online]. Available: https://www.movella.com/resources/cases/development-validation-inertial-sensor-based-human-model-integrated-compensation-errors

[18] J.-T. Zhang, A. C. Novak, B. Brouwer, and Q. Li, "Concurrent validation of Xsens MVN measurement of lower limb joint angular kinematics," *Physiological Meas.*, vol. 34, no. 8, pp. N63–N69, Aug. 2013.

[19] L. Donisi, G. Pagano, G. Cesarelli, A. Coccia, F. Amitrano, and G. D'Addio, "Benchmarking between two wearable inertial systems for gait analysis based on a different sensor placement using several statistical approaches," *Measurement*, vol. 173, Mar. 2021, Art. no. 108642.

[20] P. Puchaud et al., "Accuracy and kinematics consistency of marker-based scaling approaches on a lower limb model: A comparative study with imagery data," *Comput. Methods Biomech. Biomed. Eng.*, vol. 23, no. 3, pp. 114–125, Feb. 2020.

[21] M. E. Raabe and A. M. W. Chaudhari, "An investigation of jogging biomechanics using the full-body lumbar spine model: Model development and validation," *J. Biomech.*, vol. 49, no. 7, pp. 1238–1243, May 2016.

[22] P. Picerno et al., "Upper limb joint kinematics using wearable magnetic and inertial measurement units: An anatomical calibration procedure based on bony landmark identification," *Sci. Rep.*, vol. 9, no. 1, p. 14449, Oct. 2019.

[23] R. Dumas et al., "Adjustments to McConville and Young body segment inertial parameters," *J. Biomech.*, vol. 40, no. 3, pp. 543–553, 2007.

[24] W. H. Ho, T. Y. Shiang, C. C. Lee, and S. Y. Cheng, "Body segment parameters of young Chinese men determined with magnetic resonance imaging," *Med. Sci. Sports Exerc.*, vol. 45, no. 9, pp. 1759–1766, Sep. 2013.

[25] Y. Ma, J. Kwon, Z. Mao, K. Lee, L. Li, and H. Chung, "Segment inertial parameters of Korean adults estimated from three-dimensional body laser scan data," *Int. J. Ind. Ergonom.*, vol. 41, no. 1, pp. 19–29, Jan. 2011.

[26] S. Goel and R. Tashakkori, "Correlation between body measurements of different genders and races," *Collaborative Math. Statist. Res.*, vol. 109, pp. 7–17, 2015.

[27] I. Weygers et al., "In-vitro validation of inertial-sensor-to-bone alignment," *J. Biomech.*, vol. 128, Nov. 2021, Art. no. 110781.

[28] M. Zuk and C. Pezowicz, "Kinematic analysis of a six-degrees-of-freedom model based on ISB recommendation: A repeatability analysis and comparison with conventional gait model," *Appl. Bionics Biomech.*, vol. 2015, Jan. 2015, Art. no. 503713.

[29] R. M. Ehrig, W. R. Taylor, G. N. Duda, and M. O. Heller, "A survey of formal methods for determining the centre of rotation of ball joints," *J. Biomech.*, vol. 39, no. 15, pp. 2798–2809, 2006.

[30] M. A. Robinson and J. Vanrenterghem, "An evaluation of anatomical and functional knee axis definition in the context of side-cutting," *J. Biomech.*, vol. 45, no. 11, pp. 1941–1946, Jul. 2012.

[31] *FOHEART.X*. Accessed: Mar. 17, 2023. [Online]. Available: http://foheart.com/en/index.php/products/foheartx.html

[32] ASI Association. *Motor Exam Guide*. Accessed: Mar. 17, 2023. [Online]. Available: https://asia-spinalinjury.org/wp-content/uploads/2016/02/Motor_Exam_Guide.pdf

[33] *Supporting Material*. Accessed: Mar. 27, 2023. [Online]. Available: https://github.com/wangzhengtao1993/AnatomicalLandmarkTrajectoriesBasedonIMUData

[34] R. A. Clark, K. J. Bower, B. F. Mentiplay, K. Paterson, and Y. H. Pua, "Concurrent validity of the Microsoft Kinect for assessment of spatiotemporal gait variables," *J. Biomech.*, vol. 46, no. 15, pp. 2722–2725, Oct. 2013.

[35] Y. Zhu, W. Lu, R. Zhang, R. Wang, and D. Robbins, "Dual-channel cascade pose estimation network trained on infrared thermal image and groundtruth annotation for real-time gait measurement," *Med. Image Anal.*, vol. 79, Jul. 2022, Art. no. 102435.

[36] S. Qiu, Z. Wang, H. Zhao, and H. Hu, "Using distributed wearable sensors to measure and evaluate human lower limb motions," *IEEE Trans. Instrum. Meas.*, vol. 65, no. 4, pp. 939–950, Apr. 2016.